Volume 53
Number 2
14 January 2024
Pages 367-822

Dalton Transactions

An international journal of inorganic chemistry

rsc.li/dalton

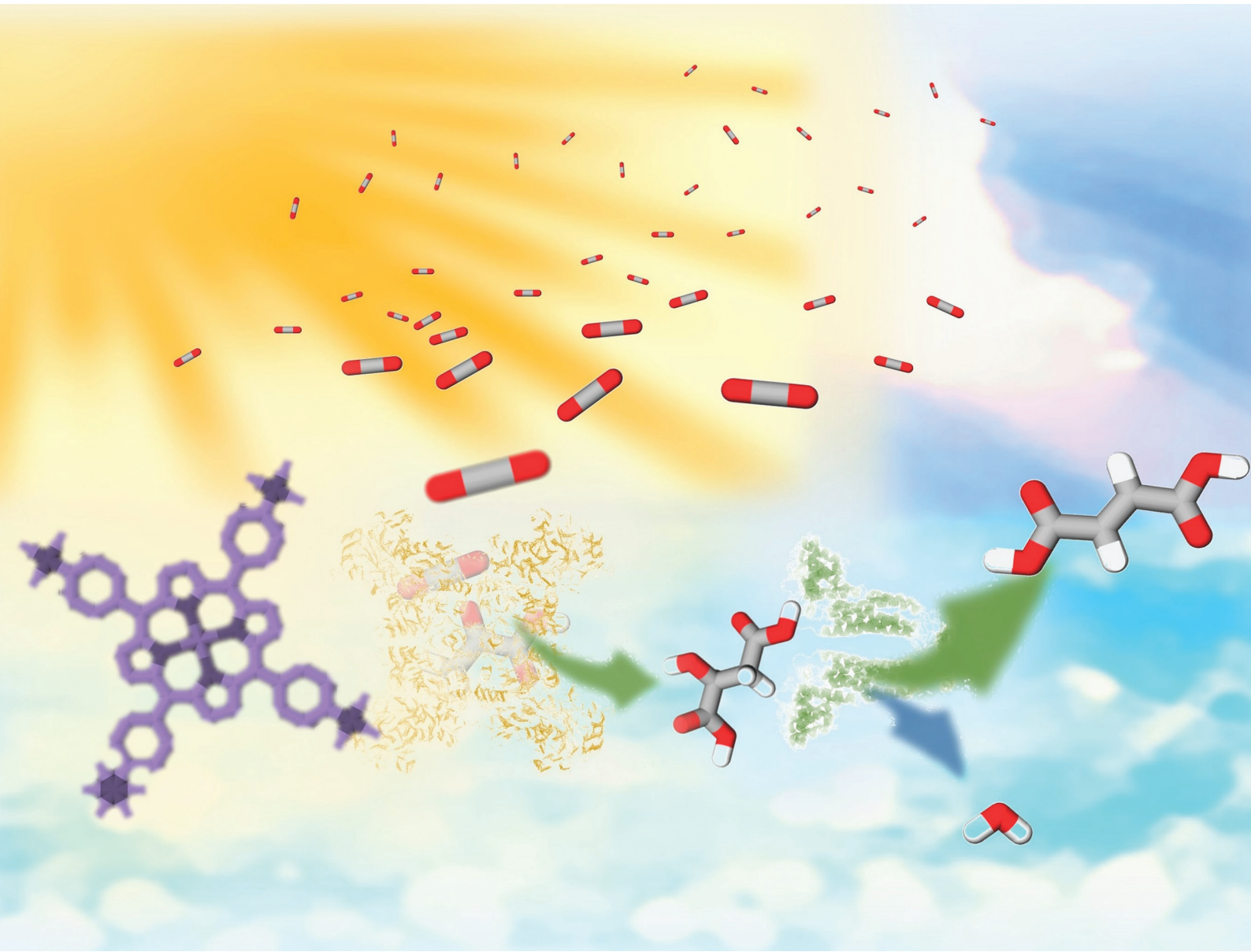

ISSN 1477-9226

ROYAL SOCIETY OF CHEMISTRY

COMMUNICATION

Mika Takeuchi and Yutaka Amao

An effective visible-light driven fumarate production from gaseous CO_2 and pyruvate by the cationic zinc porphyrin-based photocatalytic system with dual biocatalysts

Dalton Transactions

ROYAL SOCIETY OF CHEMISTRY

COMMUNICATION

View Article Online
View Journal | View Issue

Cite this: *Dalton Trans.*, 2024, **53**, 418

Received 20th October 2023,
Accepted 24th November 2023

DOI: 10.1039/d3dt03492e

rsc.li/dalton

An effective visible-light driven fumarate production from gaseous CO_2 and pyruvate by the cationic zinc porphyrin-based photocatalytic system with dual biocatalysts†

Mika Takeuchi[a] and Yutaka Amao *[a,b]

Fumaric acid is a useful unsaturated dicarboxylic acid that serves as a precursor for the biodegradable plastics poly(butylene succinate) and poly(propylene fumarate). Currently, fumaric acid is mainly synthesised from petroleum resources such as benzene. It is therefore desirable to develop methods to produce fumaric acid from renewable resources such as those derived from biomass. In this work, an effective visible-light driven fumarate production from gaseous CO_2 and pyruvate with the system consisting of triethanolamine, cationic water-soluble zinc porphyrin, zinc tetrakis (4-*N*,*N*,*N*-trimethylaminophenyl)porphyrin, pentamethylcyclopentadienyl coordinated rhodium(III) 2,2′-bipyridyl complex, NAD^+, malate dehydrogenase (NAD^+-dependent oxaloacetate-decarboxylating) and fumarase was developed.

Fumaric acid, *trans*-butenedioic acid, is the simplest dicarboxylic acid with a carbon–carbon double bond in the molecule. Fumaric acid is a chemical building block with many applications, including in the polymer materials industry.[1–3] Particularly in the field of polymer chemistry, fumaric acid is also useful as a raw material for the biodegradable plastics poly(butylene succinate) (PBS)[4] and poly(propylene fumarate) (PPF).[5] Currently, fumaric acid is synthesised mainly by petroleum-based chemical production. Conventional fumaric acid is produced by oxidising furfural with chlorate in the presence of a vanadium catalyst.[6] Limited fossil resources, rising oil prices and growing interest in the carbon cycle in chemical synthesis have led to increased interest in the development of bio-based fumaric acid from renewable resources and CO_2. Fermentation methods produce fumaric acid from glucose *via* the reductive tricarboxylic acid (TCA) pathway and were used in industry before the development of the petrochemical industry.[7] The conventional fumaric acid fermentation has problems of high costs with low product yields and productivity, and produces a wide variety of by-products. In view of these constraints, we devoted to a simple biocatalytic fumaric acid production from CO_2 and biomass-derived materials such as pyruvic acid. The biocatalytic fumarate production from bicarbonate or gaseous CO_2 and pyruvate *via* L-malate as an intermediate with dual biocatalysts (malate dehydrogenase; NAD^+-dependent oxaloacetate-decarboxylating; MDH EC 1.1.1.38) and fumarase (FUM; EC 4.2.1.2) in the presence of NADH in an aqueous media has been reported.[8,9] After 7 h incubation, the conversion yields of pyruvate to fumarate from bicarbonate or gaseous CO_2 as feedstock are estimated to be 13 or 12%, respectively. Since this system uses NADH as a sacrificial reagent, it is necessary to integrate the NAD^+ to NADH regeneration system. Thus, the visible-light driven fumarate production from pyruvate and bicarbonate or gaseous CO_2 with the combination of NAD^+ reduction to NADH system of triethanolamine (TEOA) as an electron donor, water-soluble zinc porphyrin, (ZnP) as a photosensitiser and $[Cp^*Rh(bpy)(H_2O)]^{2+}$, and dual biocatalysts (MDH and FUM) as shown in Fig. 1 also has been reported.[10,11] In this system, zinc *meso*-tetra(4-sulfonatophenyl)porphyrin tetrasodium salt ($ZnTPPS^{4-}$) was used as a photosensitiser.

By using this system, the conversion yields of pyruvate to fumarate from bicarbonate or gaseous CO_2 as feedstock are

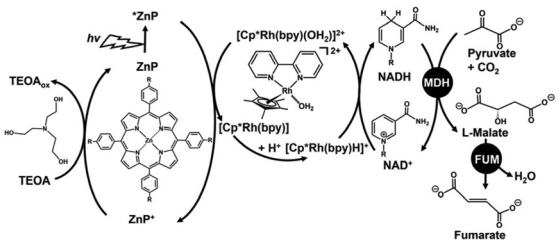

Fig. 1 Visible-light driven fumarate production from pyruvate and CO_2 with the system consisting of TEOA, water-soluble zinc porphyrin (ZnP), $[Cp^*Rh(bpy)(H_2O)]^{2+}$, NAD^+, MDH and FUM.

[a]*Graduate School of Science, Osaka Metropolitan University, 3-3-138 Sugimoto, Sumiyoshi-ku, Osaka 558-8585, Japan. E-mail: amao@omu.ac.jp*
[b]*Research Centre of Artificial Photosynthesis (ReCAP), Osaka Metropolitan University, 3-3-138 Sugimoto, Sumiyoshi-ku, Osaka 558-8585, Japan*

† Electronic supplementary information (ESI) available. See DOI: https://doi.org/10.1039/d3dt03492e

estimated to be 0.9 or 1.0% after 5 h irradiation, respectively. Using this system, fumarate could be synthesised from pyruvate and gaseous CO_2 using visible light energy as the driving force, but the yield of fumarate production remained low compared with that the non-photoredox system consisting of NADH, MDH and FUM. One of the reasons for the low efficiency of fumarate production was predicted to be the direct effect of $ZnTPPS^{4-}$ used as a photosensitiser in the visible light-driven NADH regeneration on the catalytic activity of FUM for the L-malate dehydration. It was reported that the addition of anionic water-soluble zinc porphyrin, $ZnTPPS^{4-}$ directly inhibited the catalytic activity of FUM-catalysed L-malate dehydration to produce fumarate (reduced to about 16% compared to control experiment).[12] The sulfonatophenyl-group of $ZnTPPS^{4-}$ binds to the substrate binding site of FUM, thereby inhibiting L-malate binding and decreasing fumarate production.[12] It was also reported that the catalytic activity of FUM was not affected by the addition of the cationic water-soluble zinc porphyrin, zinc tetrakis(4-*N*,*N*,*N*-trimethylaminophenyl)porphyrin ($ZnTMAP^{4+}$; chemical structure as shown in Fig. 2).[12]

In this study, the visible-light driven fumarate production from pyruvate and gaseous CO_2 with the combination of NAD^+ reduction system of TEOA, $ZnTMAP^{4+}$ and $[Cp^*Rh(bpy)(H_2O)]^{2+}$, MDH and FUM was investigated for the purpose of improving fumarate production efficiency.

$ZnTMAP^{4+}$ was prepared by refluxing metal-free $TMAP^{4+}$ with about 5 times molar equivalent of zinc acetate in the methanol solution according to the previous report.[13,14] Pentamethylcyclopentadienyl(2,2′-bipyridyl)rhodium(III) chloride ($[Cp^*Rh(bpy)(H_2O)]^{2+}$) was synthesized with $[Cp^*RhCl_2]_2$ and 2,2′-bipyridine according to a previous report.[15]

First, the optimum condition for the visible-light driven NAD^+ reduction to NADH was investigated. A solution consisting of TEOA (0.2 M), $ZnTMAP^{4+}$ (10–100 μM), $[Rh(Cp^*)(bpy)(H_2O)]^{2+}$ (10 μM) and NAD^+ (0.5 mM) in 5.0 ml of 500 mM 2-[4-(2-hydroxyethyl)-1-piperazinyl]ethanesulfonic acid (HEPES) buffer solution (pH 7.8) was deaerated by freeze–pump–thaw cycles repeated 6 times and the gas phase was introduced argon gas for 10 min. The sample solution was irradiated with a 250 W halogen lamp (Panasonic) as a visible-light source at 30.5 °C. Fig. 3 shows the concentration of $ZnTMAP^{4+}$ dependence of NADH production rate (v) with the system of TEOA, $ZnTMAP^{4+}$, $[Cp^*Rh(bpy)(H_2O)]^{2+}$ and NAD^+ in HEPES buffer solution. The concentration of NADH produced was determined by absorption spectrum change using UV-visible absorption spectroscopy (SHIMADZU, MaltiSpec-1500) with the molar coefficient at 340 nm (ε = 6.22 × 10^3 cm^{-1} M^{-1}).[16] The NADH production rate was determined from the concentration of NADH produced after 30 min of irradiation. As shown in Fig. 3, the NADH production rate increased generally linearly with increasing $ZnTMAP^{4+}$ concentrations. The NADH production rate was out of linearity under $ZnTMAP^{4+}$ concentration of 10 μM. It was reported that NADH production rate is maximized under the condition that the concentration of $[Rh(Cp^*)(bpy)(H_2O)]^{2+}$ is equivalent to that of $ZnTPPS^{4-}$. This suggests that this is a specific phenomenon under conditions of equal concentration of $ZnTMAP^{4+}$ and $[Cp^*Rh(bpy)(H_2O)]^{2+}$.

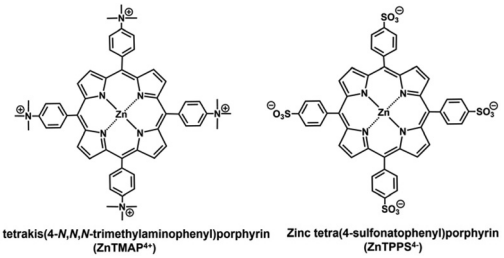

Fig. 2 Chemical structures of zinc tetrakis(4-*N*,*N*,*N*-trimethylaminophenyl)porphyrin ($ZnTMAP^{4+}$) and zinc tetra(4-sulfonatophenyl)porphyrin ($ZnTPPS^{4-}$).

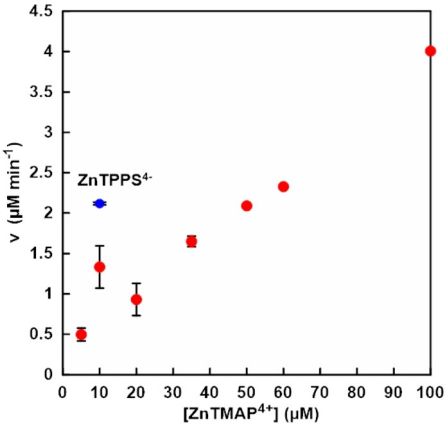

Fig. 3 The concentration of $ZnTMAP^{4+}$ dependence of NADH production rate (v) with the system of TEOA, $ZnTMAP^{4+}$, $[Cp^*Rh(bpy)(H_2O)]^{2+}$ and NAD^+ in 5.0 mL of 500 mM HEPES buffer (pH 7.8). Blue circle shows the NADH production rate (v) with the system of TEOA, $ZnTPPS^{4-}$, $[Cp^*Rh(bpy)(H_2O)]^{2+}$ and NAD^+ in 5.0 mL of 500 mM HEPES buffer (pH 7.8). Errors were obtained from the average of multiple trials.

The NADH production rate with the system of TEOA (0.2 M), $ZnTPPS^{4-}$ (10 μM), $[Cp^*Rh(bpy)(H_2O)]^{2+}$ (10 μM) and NAD^+ (0.5 mM) in HEPES buffer solution also was indicated in the Fig. 3 (blue circle). Under water-soluble zinc porphyrin concentration of 10 μM, the NADH production rate in the system with $ZnTMAP^{4+}$ was about 60% lower than that with $ZnTPPS^{4-}$. It was reported that the quantum yields of NADH production with $ZnTPPS^{4-}$ and $ZnTMAP^{4+}$ were estimated to be 1.7% and 1.1% for Soret band with 420 nm, and to be 1.3% and 1.6% for Q-band with 550 nm, respectively.[17] The molar absorption coefficients of $ZnTPPS^{4-}$ and $ZnTMAP^{4+}$ are determined to be 680 and 448 for 420 nm, and 22.1 and 18.2 cm^{-1} mM^{-1} for 550 nm, respectively.[17] Thus, these results suggested that under conditions of comparable $ZnTPPS^{4-}$ and $ZnTMAP^{4+}$ concentrations, NADH production rate are consistent with the ordinates of the molar absorption coefficients of the Soret and Q bands of the $ZnTPPS^{4-}$ and $ZnTMAP^{4+}$. From these results, it was shown that a $ZnTMAP^{4+}$ concentration of 50 μM is

required to equal the previously reported NADH production rate by a system using $ZnTPPS^{4-}$ (10 μM) as a photosensitiser. In subsequent experiments, the $ZnTMAP^{4+}$ concentration was adjusted at 50 μM.

Next let us focus on the visible-light driven L-malate production with $ZnTMAP^{4+}$ as a photosensitiser. A sample solution containing sodium pyruvate (5.0 mM), magnesium chloride (5.0 mM), TEOA (0.2 M), $ZnTMAP^{4+}$ (50 μM), $[Cp^*Rh(bpy)(H_2O)]^{2+}$ (10 μM), NAD^+ (0.5 mM) and MDH from *Sulfolobus tokodaii* purchased from Thermostable Enzyme Laboratory Co., Ltd (EC 1.1.1.38 MDH-73-01) (0.7 U; *ca.* 1.6 μM) in 5.0 mL of 500 mM HEPES–NaOH buffer (pH 7.8). The sample solution was deaerated by freeze–pump–thaw cycles repeated 6 times and then introduced in gas phase and balloon with the CO_2 gas for 10 min. The sample solution was irradiated with a 250 W halogen lamp as a visible-light source (light intensity: 200 J m^{-2} s^{-1}) at 30 °C. The reaction used an isobaric system as shown in Fig. S1.† [11] The total pressure in the reaction system was maintained at 1.01325×10^5 Pa. The system with $ZnTPPS^{4-}$ (10 μM) was used as a control experiment. Fig. S2(a)† shows the chromatogram of sodium L-malate (0–1000 μM) in 50 mM-HEPES buffer (pH 7.0). Inset of Fig. S2† shows the relationship between the L-malate concentration and the detection peak area. The L-malate concentration was calculated from the calibration curve shown in inset of Fig. S2(a)† using the eqn (S1).† After 1 h irradiation, 56.0 μM of L-malate was produced with the system of sodium pyruvate, magnesium chloride, TEOA, $ZnTMAP^{4+}$, $[Cp^*Rh(bpy)(H_2O)]^{2+}$, NAD^+ and MDH in gas phase and balloon with the CO_2 gas. On the other hand, 43.2 μM of L-malate was produced with the system using $ZnTPPS^{4-}$. There was no significant difference between both systems with $ZnTMAP^{4+}$ and $ZnTPPS^{4-}$ in the concentration of L-malate production after 1 h irradiation. Fig. 4 shows the concentration of L-malate production using $ZnTMAP^{4+}$ or $ZnTPPS^{4-}$ after 5 h irradiation (the ion chromatograph chart during the reaction is shown in Fig. S3 and S4†).

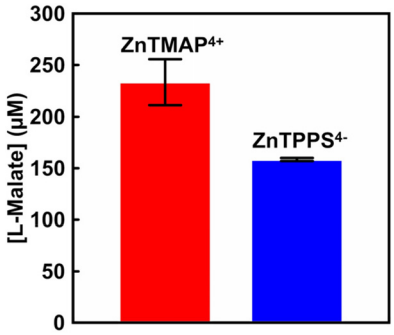

Fig. 4 The concentration of L-malate production in the system of sodium pyruvate, magnesium chloride, TEOA, $[Cp^*Rh(bpy)(H_2O)]^{2+}$, NAD^+, MDH and CO_2 gas in the presence of $ZnTMAP^{4+}$ (red) or $ZnTPPS^{4-}$ (blue) after 5 h irradiation. Errors were obtained from the average of multiple trials.

As shown in Fig. 4, 233.4 (±22.2) μM of L-malate was produced with the system of sodium pyruvate, magnesium chloride, TEOA, $ZnTMAP^{4+}$, $[Cp^*Rh(bpy)(H_2O)]^{2+}$, NAD^+ and MDH in gas phase and balloon with the CO_2 gas after 5 h irradiation. However, 158.5 (±1.5) μM of L-malate was produced with the system using $ZnTPPS^{4-}$. By using $ZnTMAP^{4+}$ as a photosensitiser, approximately 1.5 times more L-malate was produced than in the system with $ZnTPPS^{4-}$. For the system using $ZnTMAP^{4+}$, the L-malate production rates after 1 and 5 h irradiation were estimated to be 56.0 and 46.7 μM h^{-1}, respectively. For the system using $ZnTPPS^{4-}$, the production rates after 1 and 5 h irradiation were estimated to be 43.7 and 31.7 μM h^{-1}, respectively. The rate of L-malate production gradually decreased with irradiation time in the system with $ZnTPPS^{4-}$. In contrast, no decrease in the rate of L-malate production with irradiation time was observed in the system with $ZnTMAP^{4+}$. We have reported stable NAD^+ reduction NADH in a system of TEOA and $[Cp^*Rh(bpy)(H_2O)]^{2+}$ with $ZnTMAP^{4+}$ as a photosensitiser compared to a system using anionic water-soluble zinc porphyrins such as $ZnTPPS^{4-}$.[17] Thus, it was found that the efficiency of visible-light driven L-malate production was improved by using $ZnTMAP^{4+}$ as a photosensitiser.

Finally, visible-light driven fumarate production from pyruvate and gaseous CO_2 was investigated using the system of with the addition of FUM from porcine heart purchased from Merck Co., Ltd (EC 4.2.1.2; molecular weight: 200 kDa)[18] (details of the experiment are described in ESI†). A sample solution containing sodium pyruvate (5.0 mM), magnesium chloride (5.0 mM), TEOA (0.2 M), $ZnTMAP^{4+}$ (50 μM), $[Cp^*Rh(bpy)(H_2O)]^{2+}$ (10 μM), NAD^+ (0.5 mM), MDH (0.7 U; *ca.* 1.6 μM) and FUM (0.5 U; *ca.* 1.3 nM) in 5.0 mL of 500 mM HEPES–NaOH buffer (pH 7.8). The sample solution was deaerated by freeze–pump–thaw cycles repeated 6 times and then introduced in gas phase and balloon with the CO_2 gas for 10 min. The sample solution was irradiated with a 250 W halogen lamp as a visible-light source (light intensity: 200 J m^{-2} s^{-1}) at 30 °C. The reaction used an isobaric system as shown in Fig. S1.† The total pressure in the reaction system was maintained at 1.01325×10^5 Pa. The system with $ZnTPPS^{4-}$ (10 μM) also was used as a control experiment. The concentration of fumarate produced was measured by an ion chromatography. Fig. S2(b)† shows the chromatogram of sodium fumarate (0–1000 μM) in 50 mM-HEPES buffer (pH 7.0). The inset of Fig. S2(b)† shows the relationship between the fumarate concentration and the detection peak area. The fumarate concentration was calculated from the calibration curve shown in inset of Fig. S3† using the eqn (S2).† After 1 h irradiation, 13.2 μM of fumarate was produced with the system of sodium pyruvate, magnesium chloride, TEOA, $ZnTMAP^{4+}$, $[Cp^*Rh(bpy)(H_2O)]^{2+}$, NAD^+, MDH and FUM in gas phase and balloon with the CO_2 gas. In contrast, 9.2 μM of fumarate was produced with the system using $ZnTPPS^{4-}$. By using $ZnTMAP^{4+}$ as a photosensitiser, approximately 1.4 times more fumarate was produced than in the system with $ZnTPPS^{4-}$. Fig. 5 shows the concentration of fumarate production using

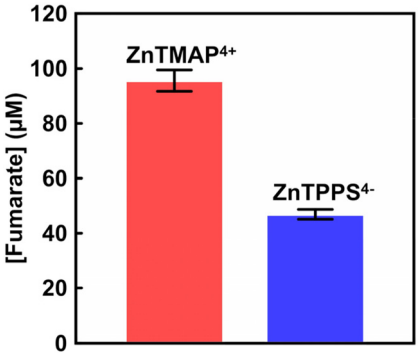

Fig. 5 The concentration of fumarate production in the system of sodium pyruvate, magnesium chloride, TEOA, $[Cp^*Rh(bpy)(H_2O)]^{2+}$, NAD^+, MDH, FUM and CO_2 gas in the presence of $ZnTMAP^{4+}$ (red) or $ZnTPPS^{4-}$ (blue) after 5 h irradiation. Errors were obtained from the average of multiple trials.

$ZnTMAP^{4+}$ or $ZnTPPS^{4-}$ after 5 h irradiation (the ion chromatograph chart during the reaction is shown in Fig. S5 and S6†). As shown in Fig. 5, 96.9 (±3.9) μM of fumarate was produced with the system using $ZnTMAP^{4+}$ after 5 h irradiation. However, 46.9 (±1.8) μM of fumarate was produced with the system using $ZnTPPS^{4-}$. By using $ZnTMAP^{4+}$, approximately 2.0 times more fumarate was produced than in the system with $ZnTPPS^{4-}$. Let's now discuss the argument based on the catalytic efficiency of the FUM in both systems using $ZnTMAP^{4+}$ and $ZnTPPS^{4-}$. For the system using $ZnTMAP^{4+}$, the turnover number (TON) and turnover frequency (TOF) of FUM (1.3 nM) were estimated to be 76 769 and 4.3 s^{-1}, respectively. For the system using $ZnTPPS^{4-}$, in contrast, TON and TOF of FUM were calculated to be 37 462 and 2.0 s^{-1}, respectively. Furthermore, 41.0 μM of fumarate was produced in the system with 5-fold equivalent amounts of $ZnTPPS^{4-}$ (50 μM) (the ion chromatograph chart during the reaction is shown in Fig. S7†). Under $ZnTPPS^{4-}$ concentrations of 10 and 50 μM, 191 and 339 μM L-malate were produced as the intermediate after 5 h of irradiation, respectively. No increase in fumarate production was observed under the condition of increased $ZnTPPS^{4-}$ concentrations, even though more of the intermediate L-malate was produced. After 5 h irradiation, the present ratio of L-malate and fumarate under $ZnTPPS^{4-}$ concentrations of 10 and 50 μM was calculated to be 0.25 and 0.12, respectively. These results suggest that $ZnTPPS^{4-}$ also directly inhibits the catalytic activity of FUM in the visible-light driven fumarate production with the system of sodium pyruvate, magnesium chloride, TEOA, $ZnTPPS^{4-}$, $[Cp^*Rh(bpy)(H_2O)]^{2+}$, NAD^+, MDH and FUM in the presence of gaseous CO_2. Meanwhile, 313 μM of L-malate was produced as the intermediate after 5 h of irradiation using $ZnTMAP^{4+}$ (50 μM). After 5 h irradiation, the present ratio of L-malate and fumarate was calculated to be 0.30. The results indicate that $ZnTMAP^{4+}$ acts only as a photosensitiser for visible light-driven NADH and is not involved in the catalytic activity of FUM. By using $ZnTMAP^{4+}$ as a photosensitiser, therefore, an effective visible-light driven fumarate production from gaseous CO_2 and pyruvate with MDH and FUM was accomplished.

In this system, fumarate production has been observed up to 24 h of irradiation; MDH is a thermostable enzyme and durable to prolonged use, so the reaction can proceed again with the addition of pyruvate, whereas FUM shows decreased catalytic activity for longer reaction. This means that the addition of FUM after a certain irradiation time is expected to extend the lifetime of the reaction system.

In conclusion, we have successfully improved the efficiency of visible-light driven fumarate production from pyruvate and gaseous CO_2 by using $ZnTMAP^{4+}$ as a photosensitiser in the system combination of NAD^+ reduction with $[Cp^*Rh(bpy)(H_2O)]^{2+}$ and dual biocatalysts (MDH and FUM) in the presence of TEOA (approximately 2.0 times more fumarate is produced than in the system using $ZnTPPS^{4-}$, conventionally photosensitizer). The use of $ZnTMAP^{4+}$ increased the yield of fumarate production from pyruvate and CO_2 without interfering with the catalytic activity of FUM, coupled with the effect of also increasing the yield of visible light driven L-malate production using MDH as a catalyst.

Conflicts of interest

There are no conflicts to declare.

Acknowledgements

This work was partially supported by Grant-in-Aid for Specially promoted Research (23H05404), Scientific Research (B) (22H01872), (22H01871) and Fund for the Promotion of Joint International Research (Fostering Joint International Research (B)) (19KK0144), and by Institute for Fermentation, Osaka (IFO) (G-2023-3-050).

Notes and references

1 A. Pellis, A. E. Herrero, L. Gardossi, V. Ferrario and G. M. Guebitz, *Polym. Int.*, 2016, **65**, 861.
2 N. A. Rorrer, J. R. Dorgan, D. R. Vardon, C. R. Martinez, Y. Yang and G. T. Beckham, *ACS Sustainable Chem. Eng.*, 2016, **4**, 6867.
3 Y. Jiang, A. J. J. Woortman, G. O. R. Alberda van Ekenstein and K. Loos, *Polym. Chem.*, 2015, **6**, 5451.
4 N. Jacquel, F. Freyermouth, F. Fenouillot, A. Rousseau, J. P. Pascault, P. Fuertes and R. Saint-Loup, *J. Polym. Sci., Part A: Polym. Chem.*, 2011, **49**, 5301.
5 S. He, M. D. Timmer, M. J. Yaszemski, A. W. Yasko, P. S. Engel and A. G. Mikos, *Polymer*, 2001, **42**, 1251.
6 J. Shao, Y. Ni and L. Yan, *J. Bioresour. Bioprod.*, 2021, **6**, 39.
7 V. Martin-Dominguez, J. Estevez, F. De Borja Ojembarrena, V. E. Santos and M. Ladero, *Fermentation*, 2018, **4**, 33.
8 M. Takeuchi and Y. Amao, *React. Chem. Eng.*, 2022, **7**, 1931.
9 M. Takeuchi and Y. Amao, *RSC Sustainability*, 2023, **1**, 90.

10 M. Takeuchi and Y. Amao, *Sustainable Energy Fuels*, 2023, **7**, 355.
11 M. Takeuchi and Y. Amao, *RSC Sustainability*, 2023, **1**, 1874.
12 M. Takeuchi and Y. Amao, *New J. Chem.*, 2023, **47**, 17679.
13 K. Kalyanasundaram and M. Neumann-Spallart, *J. Phys. Chem.*, 1982, **86**, 5163.
14 K. Kalyanasundaram, *J. Chem. Soc., Faraday Trans. 2*, 1983, **79**, 1365.
15 U. Kölle, B. S. Kang, P. Infelta, P. Comte and M. Grätzel, *Chem. Ber.*, 1989, **122**, 1869.
16 R. B. McComb, L. W. Bond, R. W. Burnett, R. C. Keech and G. N. Bowers Jr., *Clin. Chem.*, 1976, **22**, 141.
17 M. Takeuchi and Y. Amao, *Bull. Chem. Soc. Jpn.*, 2023, **96**, 1206.
18 S. Beeckmans and E. Van Driessche, *J. Biol. Chem.*, 1998, **273**, 31661.